Scientific Reports

https://doi.org/10.1038/s41598-026-42614-9

Article in Press

Microstructure and mechanical properties of (Mg, Ce)-modified Al-7.5Si-15Cu-5Zn brazing joints on 5083 aluminum alloy

Received: 17 October 2025

Accepted: 26 February 2026

Published online: 05 March 2026

Cite this article as: Wang Y., Zhuo Y., Sun Z. *et al.* Microstructure and mechanical properties of (Mg, Ce)-modified Al-7.5Si-15Cu-5Zn brazing joints on 5083 aluminum alloy. *Sci Rep* (2026). https://doi.org/10.1038/s41598-026-42614-9

Yan Wang, Yuechao Zhuo, Zhe Sun, Conghui Zhang, Yonglin Zhao, Bingyuan Han & Yuxiang Liu

Microstructure and Mechanical Properties of (Mg, Ce)-Modified Al-7.5Si-15Cu-5Zn Brazing Joints on 5083 Aluminum Alloy

Yan Wang[1], Yuechao Zhuo[2], Zhe Sun[3], Conghui Zhang[4], Yonglin Zhao[4*], Bingyuan Han[4], Yuxiang Liu[5*]

1. School of Civil Engineering and Transportation, Northeast Forestry University, Harbin 150040, China;

2. School of Automotive and Traffic Engineering, Jiangsu University of Technology, Chang Zhou 213001, China;

3. National Key Laboratory for Remanufacturing, Beijing 100072, China

4. Hubei Provincial Key Laboratory of Automotive Power Transmission and Electronic Control, Shiyan 442002, China;

5. Research Centre for Laser Extreme Manufacturing, Ningbo Institute of Materials Technology and Engineering, Chinese Academy of Sciences, Ningbo 315201, China.

*Corresponding author: Yonglin Zhao E-mail address: zhaoyonglin0428@163.com.

Yuxiang Liu E-mail address: liuyuxiang@nimte.ac.cn.

Abstract: This study investigated the microstructural evolution of Al-7.5Si-15Cu-5Zn brazing alloys modified by adding 0.5 wt.% Mg and xCe (x=0.05 wt.%, 0.1 wt.%, 0.2 wt.%, 0.3 wt.%, 0.4 wt.%) . The mechanical properties of the corresponding brazing joints on 5083 aluminum alloy were measured with the aid of first-principle calculations. Results show that Mg and Ce elements refine the microstructure of Al-7.5Si-15Cu-5Zn brazing alloys by changing the morphology of the intermetallic phases. There is an interface zone

between the brazing alloy and the base alloy in the joints and the thickness of interface zone evolves with the Mg addition and Ce contents. The virtual crystal approximation (VCA) method predicts the best mechanical properties of the joints using Al-7.5Si-15Cu-5Zn-0.5Mg-0.2Ce brazing alloy, exhibiting the measured tensile strength, elongation and microhardness of 261.14 MPa, 11.95 % and 194.6 $HV_{0.2}$, respectively. Compared to the base brazing alloy without Mg and Ce additions, the tensile strength is increased by 42% and the elongation is improved by 47%.

Keywords: Aluminum alloy brazing; brazed joints; microstructure and phases, First-principles calculation; Mechanical properties

1 Introduction

Aluminum alloys are widely used in automotive, marine, and aerospace applications due to their high specific strength and excellent corrosion resistance[1],[2]. However, to ensure their long-term service in complex environments, reliable repair methods are required after cracking or fracture damage occurs. Brazing technology, characterized by a small heat-affected zone and the fact that the base material does not melt, is currently one of the important methods for joining aluminum alloys[3][4]. Thus, this technology is suitable to weld Al alloys with low melting points to achieve effective repair without sacrificing mechanical properties.

For 5083 aluminum alloy, it has a low melting point of 574 ℃ and the hypoeutectic Al-Si alloys (Si, ≤12.6 wt.%) are the common brazing alloys to weld it. Though hypoeutectic Al-Si alloys possess excellent wettability and fluidity, the high eutectic point (588.12 °C) makes it difficult to effectively braze 5083 aluminum alloy[5][6]. Furthermore, massive Si particles and tightly elongated Al-Si eutectic phases exist in Al-Si alloys prepared by conventional casting

after solidification. Such phases might induce stress concentration to degrade the tensile strength of the alloy[7][8]. To achieve a better solderability of Al-Si brazing alloy and good properties of 5083 Al alloy joints, elements such as Ge, Cu, and Zn have been added to form low-melting-point eutectics with Al[9][11]. For Al-Ge binary alloy, its eutectic point is 423 ℃ when Ge content reaches 51.6 wt.%, which seems to be a good composition if Ge is added in Al-Si alloy. However, Ge can react with Si to form brittle Si-Ge phases which make the brazing alloy brittle to degrade the machinability. The solubility of Zn in α-Al is relatively high and an appropriate amount of Zn dissolved in Al can strengthen the mechanical properties of the alloy and improve its tensile strength[12]. For Al-Si-Cu alloy, a ternary eutectic (eutectic point 525 °C) forms at a Cu content of 26.7 wt.% and a Si content of 5.1 wt.%. With a bigger Cu content, the properties of Al-Si brazing alloy is enhanced and the melting point decreases. However, the brittle Al_2Cu phases form with excessive Cu addition, lowering the mechanical properties of the brazed joint[13].

Therefore, Al-Si-Cu-Zn alloy is well developed and investigated in some studies to be used as brazing alloy[14][16]. To further mitigate the impact of brittle phases on Al-Si brazing alloys, elements such as Mg and Ce are further added to refine the microstructure. Li et al.[17] found that the addition of Mg in Al-Si alloy reduced the surface tension of liquid metal and improves its fluidity. Musa et al.[18] reported that at an Mg content of 0.67 wt.%, the solidified Al-Si-Mg alloy exhibited a uniform microstructure, reduced porosity, and optimal mechanical properties. Ye et al.[19] discovered that adding Ce to Al-7Si alloys refined α-Al grains and reduced the size of Si particles. Sezgin et al.[20]found that an appropriate amount of Ce to Al-12Si alloys contributed to refinement of intermetallic compounds. In addition, it has been reported that

rare-earth elements often exhibit a more pronounced modification effect when co-added with other modifier elements[21][22]. Overall, adding Mg and Ce in Al-Si-Cu-Zn alloy is capable of refining the microstructure and imporving the mechanical properties, possibly making the Al-Si-Cu-Zn-Mg-Ce alloy an excellent brazing alloy.

In this study, a low-melting-point brazing alloy with high-strength is developed by adding 0.5 wt.% Mg and xCe (x = 0.05 wt.%, 0.1 wt.%, 0.2 wt.%, 0.3 wt.%, 0.4 wt.%) in Al-7.5Si-15Cu-5Zn alloy to braze 5083 aluminum alloy. Based on the hypoeutectic Al–7.5Si alloy, 15 wt.% Cu was introduced to reduce the melting temperature and 5 wt.% Zn was added to strengthen the filler. On this basis, Mg and Ce were further introduced to refine the microstructure of the base brazing alloy, thereby improving the mechanical performance of the corresponding joints. The evaluation of mechanical properties of these alloy with different Ce, first-principle calculations were adopted. However, there is no consensus on the modeling method for multicomponent alloys calculations. Common methods include Similar Local Atomic Environment (SLAE), Special Quasirandom Structure (SQS), Coherent Potential Approximation (CPA), and Virtual Crystal Approximation (VCA)[23]. Among them, SLAE and SQS require a construction of ultra-small regions, resulting in high computational costs for multicomponent alloys. CPA assumes ideal lattice sites for atoms, ignoring the effects of lattice distortions. VCA simplifies the complex structures caused by atomic substitutions, making modeling straightforward and computationally efficient, particularly for predicting the elastic properties of multicomponent alloys[24]4[26]. For example, Chen et al.[26] used the VCA method to calculate the lattice constants and elastic properties of the refractory high-entropy alloy Ti_xVNbMo (x=1.00, 1.25, 1.50, 2.00). Comparisons with experimental results confirmed the validation of

the VCA method.

In this work, a VCA model for the multicomponent Al-7.5Si-15Cu-5Zn-0.5Mg-xCe brazing alloy system was established. First-principle calculations were used to predict the influences of Mg addition and Ce contents on the mechanical properties. Meanwhile, microstructure characterizations and property measurements were carried out to investigate the Mg and Ce influences on the brazed joints.

2 Materials and methods

2.1 Brazing alloys preparation

Ingots of Al with a purity of 99.99 %, along with Al-12Si, Al-20Cu, and Al-10Ce master alloys, were melted in an SX2-4-10A box-type resistance furnace at 750 °C, followed by cooling to 650 °C to add Mg and Zn elements. The complete melt was thoroughly stirred to minimize segregation of the elements. The melt was then poured into molds and cooled in air. The solidified brazing alloy ingots were hot-rolled at 420 °C to a thickness of 3 mm. The chemical compositions of the brazing alloys are shown in Table 1.

Table 1. Chemical compositions of brazing alloys (wt.%).

Sample number	Al	Si	Cu	Zn	Mg	Ce
1	Bal.	7.5	15	5	—	—
2	Bal.	7.5	15	5	0.5	—
3	Bal.	7.5	15	5	0.5	0.05
4	Bal.	7.5	15	5	0.5	0.1
5	Bal.	7.5	15	5	0.5	0.2
6	Bal.	7.5	15	5	0.5	0.3
7	Bal.	7.5	15	5	0.5	0.4

The brazing alloy samples were cut and processed using an

electrical discharge machining (EDM) machine. The melting temperature was measured using a differential scanning calorimeter (DSC). The microstructure were characterized using a scanning electron microscope (SEM) equipped with energy-dispersive X-ray spectroscopy (EDS). The phases were analyzed using an X-ray diffractometer (XRD).

The melting behavior of the brazing alloys was characterized by differential scanning calorimetry (DSC). Approximately 0.15 g of each sample was sealed in an Al_2O_3 crucible, and heated at a constant rate of 25 °C/min under a protective argon atmosphere (mL/min). Prior to testing, the DSC was calibrated for temperature by the testing facility according to the manufacturer's procedure using certified reference materials. The onset and peak temperatures were determined using the tangent method from the DSC curves.

2.2 Brazing process

The chemical compositions of the 5083 aluminum alloy sheet used in the brazing experiment is shown in Table 2. The sheet dimensions are 200 mm × 100 mm × 3 mm. The alloy was prefabricated with an artificial fissure with 150 mm × 2 mm × 2 mm. Before the brazing experiment, the alloy surfaces were polished with sandpaper and cleaned with anhydrous ethanol to remove oil and contamination. Under the protection of inert gas (argon), tungsten inert gas arc welding (TIG) was used as the heat source for brazing. During the experiment, the arc was ignited for 2-3 seconds. Then, the surface oxide layer of the base material was removed using a negative-cycle high-frequency AC arc before filling the weld seam with brazing alloy. The welding current was 100 A, the distance between the tungsten electrode and the base material surface was

10 mm, the torch travel speed was 3 mm/s, and the argon shielding gas flow rate was 15 L/min. The schematic diagram of the arc brazing process is shown in Fig. 1.

Table 2. Chemical composition of 5083 aluminum alloy (wt.%).

5083	Si	Fe	Cu	Mn	Mg	Cr	Zn	Ti	Al
	0.4	0.4	0.1	0.4-1.0	4.0-4.9	0.02	0.25	0.15	Bal.

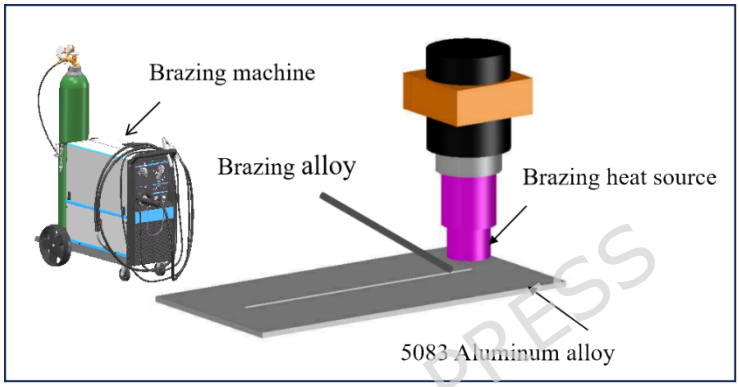

Fig. 1 Schematic diagram of arc brazing

After brazing, one metallographic specimen and three tensile specimens were extracted from the mid-length of the brazed seam (excluding the arc start/stop regions). Using an electrical discharge machining (EDM) machine, as schematically shown in Fig. 2. The tensile tests were conducted in accordance with the Chinese standard GB/T 11363-2008 (Test method of the strength for brazed joint). Tensile tests were performed on the joints using a universal testing machine, and three specimens were tested for each condition. The microstructure of the brazed joint was characterized using SEM equipped with EDS.

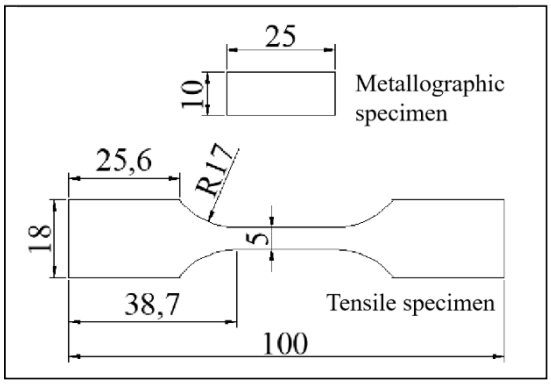

Fig. 2 Metallographic and tensile specimens (Unit: mm)

2.3 First-principle calculations

2.3.1 First-principle model

The first-principle calculations based on density functional theory (DFT) were performed using the Cambridge Sequential Total Energy Package (CASTEP) module within the Materials Studio program[27]. Fig. 3 shows the FCC (face-centered cubic) structure model of the Al-7.5Si-15Cu-5Zn-0.5Mg-xCe multicomponent brazing alloy, which is constructed using the VCA method[28]. In Fig. 3, each atom represents a mixture of alloy atoms, meaning that each atom encompasses all the atoms present in the brazing alloy. Total energy of electronic structure was calculated using norm-conserving pseudopotentials proposed by Vanderbilt and PBE (Perdu-Burke-Ernzerhof) functional form within framework of General Gradient Approximation[29]. Based on the convergence test of cutoff energy and k-points using the Monkhorst-Pack method, a plane-wave basis set with a cutoff energy of 900 eV was used to expand the electronic wave functions, and a k-point grid of 16 × 16 × 16 was employed. The convergence criteria for geometric optimization were set as follows: the force on a single atom did not exceed 0.05 eV/Å, the maximum stress error was limited to 0.1 GPa, the maximum displacement error was constrained to 0.002 Å, and the energy per atom was less than 2.0×10^{-6} eV/atom, ensuring reliable optimization

of atomic positions and relaxation dimensions.

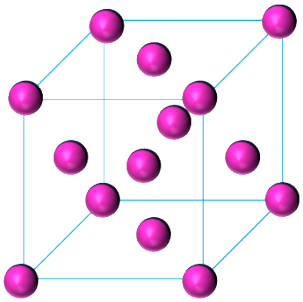

Fig. 3 Model diagram of Al-7.5Si-15Cu-5Zn-0.5Mg-xCe brazing alloy

2.3.2 Elastic constant analysis

The elastic constants (C_{ijkl}, i, j represents the directions of stress; k, l represents the directions of strain) of multicomponent brazing alloys describe the stress required to maintain a given deformation and can be expressed as follows[30]:

$$C_{ijkl} = \left(\frac{\partial \sigma_{ij}(x)}{\partial e_{kl}}\right)_X \quad (1)$$

where σ_{ij} represents the applied stress, e_{kl} represents the strain, and X and x denote the coordinates before and after deformation, respectively. For cubic crystals, three independent elastic constants (C_{11}, C_{12} and C_{44}) can be yielded from this equation. Other parameters related to the elastic constants include the bulk modulus (B), Young's modulus (E), shear modulus (G), and Poisson's ratio (v). The relationships are as follows:

$$B = B_V = B_R = (C_{11} + 2C_{12})/3 \quad (2)$$

$$G_V = (C_{11} - C_{12} + 3C_{44})/5 \quad (3)$$

$$G_R = 5(C_{11} - C_{12})C_{44}/[4C_{44} + 3(C_{11} - C_{12})] \quad (4)$$

$$G = (G_V + G_R)/2 \quad (5)$$

$$E = 9BG/(3B + G) \quad (6)$$

$$v = (3B - E)/6B \quad (7)$$

Where V represents the rigid boundary, and R represents the

flexible boundary.

The elastic modulus varies with crystallographic directions, so that the anisotropy is a critical characteristic of crystals to evaluate the elastic properties. The anisotropic behavior of the brazing alloy can be represented by the anisotropy index (A_u), which can be calculated by the following equation by MATLAB:

$$A_u = \frac{2C_{44}}{C_{11}-C_{12}} \quad (8)$$

3 Results and discussion

3.1 DSC results of brazing alloys

Fig. 4 shows the DSC melting curves of seven brazing alloys and the melting intervals. In Fig. 4 (a), the melting range of the Al-7.5Si-15Cu-5Zn brazing alloy is between 452.8 °C and 521.1 °C, with a melting interval of 68.3 °C. With the addition of 0.5 wt.% Mg, the melting point of the alloy decreases to 519.9 °C and the melting interval is reduced to 59.7 °C. The smaller melting interval indicates that Mg can slightly decrease the melting point of Al-7.5Si-15Cu-5Zn brazing alloy. With 0.05-0.2 wt.% Ce addition to the Al-7.5Si-15Cu-5Zn-0.5Mg alloy, the melting point and melting interval further decrease. At 0.2 wt.% Ce, the melting point and interval reaches the lowest values at 515.8 °C and 49.1 °C, respectively. At higher Ce content, the brazing alloy exhibits two endothermic peaks, corresponding to the Al-Si-Cu and Al-Si-Ce ternary eutectic temperatures [31]. The phase with the higher eutectic temperature results in a broader melting range for the brazing alloy, as illustrated in Fig. 4(b). For brazing alloys, a narrower melting interval indicates better flowability[32], so it can be concluded that the addition of 0.5 wt.% Mg and 0.2 wt.% Ce is capable of improving the flowability of the Al-7.5Si-15Cu-5Zn brazing alloys to enhance brazing quality.

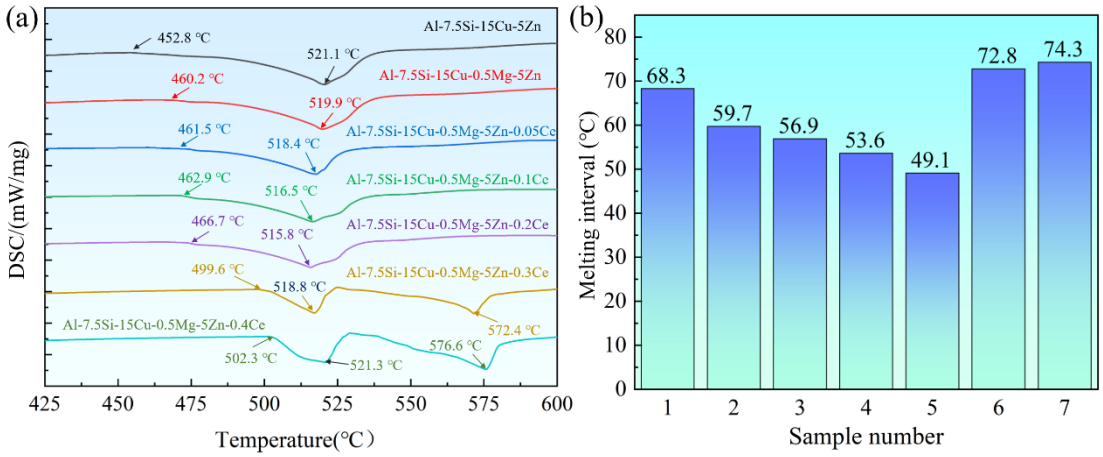

Fig. 4 (a) Melting curve of brazing alloys; (b) Melting interval of brazing alloys

3.2 Microstructure of brazing alloys

Fig. 5 shows the XRD spectra of the brazing alloys. The Al-7.5Si-15Cu-5Zn brazing alloy is composed of Al_2Cu phases, primary Si phases, Al-Si eutectic phase, Al-Zn phases in addition to the α-Al phases in the matrix. The phases are the same for the brazing after introduction 0.5 wt.% Mg. After introducing Ce, the Al-Zn phases disappear and Al_3Ce phases form. When the Ce content exceeds 0.2 wt.%, $Al_7Si_{3.5}Cu_{3.5}Ce$ phases emerges within the microstructure.

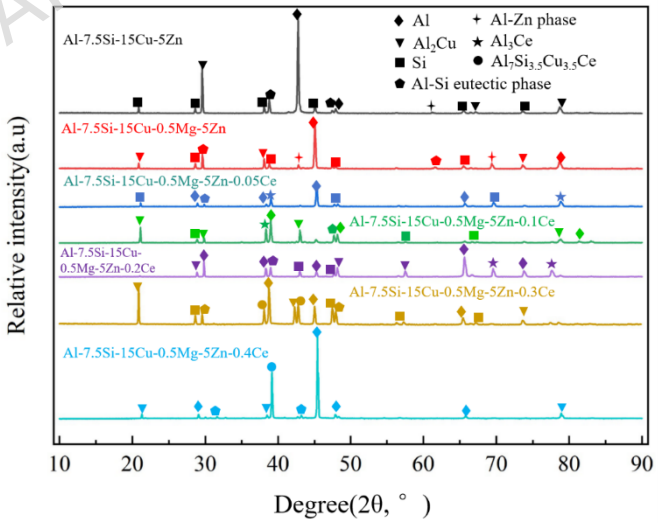

Fig. 5 XRD analysis results of brazing alloys

Fig. 6 shows the SEM morphology of the seven brazing alloys, and the EDS analysis results of points P1-P13 marked in the figure

are presented in Table 3. The Al-7.5Si-15Cu-5Zn brazing alloy exhibits gray Al_2Cu phases, black coarse Si particles, bright Al-Zn phase, and compact strip-like Al-Si eutectic phase, corresponding to the EDS analysis results of P1 to P4 in Table 3. Al_2Cu is the main secondary phase and takes over a large area. Al-Zn phases (P3) precipitates out of the Al_2Cu phases and only accounts for a very small fraction. These large block-like Si particles are embedded in the α-Al phases and are interconnected via the strip-like Al-Si eutectic phases. The Si particles exist in all brazing alloys, and representative Si particles are highlighted in the yellow boxes A–F in Fig. 6.

The size of Si particles was measured using Image-Pro software at points A–F in Fig. 6, where the particle size is defined as the equivalent circular diameter of each Si particle. The dimensions of all visible Si particles in the images were calculated, and the results are presented in Fig. 6(h). For the Al-7.5Si-15Cu-5Zn brazing alloy, the average Si particle size is 21.17 μm. When 0.5 wt.% Mg is added, the brazing alloy has the similar microstructure compared with the Al-7.5Si-15Cu-5Zn alloy with an decreased average Si particle size of 19.15 μm. Additionally, the amount of the Al-Si eutectic phases decrease, indicating more Si elements dissolve in the solid solution. This is because the atomic radius of Mg (1.36 Å) is larger than that of Al (1.18 Å), which expands the Al lattice during solidification, increasing the solubility of Si in α-Al. The above results show that Mg can refine the Si particles and the Al-Si eutectic phases, leading to a more uniform microstructure of the brazing alloy.

When 0.05 wt.% Ce was added to the Al-7.5Si-15Cu-5Zn-0.5Mg brazing alloy, the bright Al-Zn phases disappears. The introduction of Ce in the alloy promotes the formation of a new phase of Al_3Ce (P7) Fig. 6 (c). It is reported that Ce tends to form Al_3Ce phase with

Al, consuming the surrounding α-Al phase[33]. In addition, the number of Si particles decreased significantly, with only a few large Si particles remained in the α-Al phase. Meanwhile, the Al-Si eutectic phase is further refined. When the Ce content is below 0.2 wt.%, the microstructure of the brazing alloy shows no significant changes compared to that with 0.05 wt.% Ce.

At the Ce content of 0.2 wt.%, the average size of Si particles reaches the smallest at 14.34 μm. All the secondary phases are refined and show a uniform distribution. Such refinement can be attributed to that Ce is highly reactive and accumulates at the solid-liquid interface during solidification, increasing compositional undercooling, inhibiting the nucleation of the intermetallic phases. At this Ce content, the Al-Si eutectic phase is in the dot shape (P8) and discontinuously distributed in the brazing alloy. When Ce contents are bigger than 0.2 wt%, the elongated needle-like structures (P9 and P10) appear in the brazing alloy, as shown in Fig. 6 (f) and (g). These structures are composed of $Al_7Si_{3.5}Cu_{3.5}Ce$ phases (Fig. 5). The amount of needle-like phases increase with Ce content whereas the Al_2Cu phases (P12) exhibit a dramatic decline in amount. Interestingly, the Al-Si eutectic phases (P11) reprecipitate at high Ce contents, suggesting excessive Ce might coarsen the eutectic.

The evolution of microstructure and phases in Fig. 5 and Fig. 6 reflects the stability and solubility of phases, which can be explained by the the interaction strength ($W_{A\text{-}B}$) between two solvent elements A and B. $W_{A\text{-}B}$ can be expressed by[34]:

$$W_{A\text{-}B} = [\frac{\frac{R_A - R_B}{R_B}}{0.15}]^2 + [(N_A - N_B)/0.4]^2 \quad (9)$$

Where R and N represent the atomic radius and electronegativity of A and B atoms, respectively. For the Al-7.5Si-

15Cu-5Zn-0.5Mg-0.2Ce brazing alloy, $W_{Ce\text{-}M}$ (M=Al, Si, Cu, Zn, Mg) is 7.041, 11.433, 9.517, 4.275 and 3.092, respectively. Accordingly, Ce reacts easily with Al, Si and Cu to form the $Al_7Si_{3.5}Cu_{3.5}Ce$ phases. On the other hand, due to the consumption of a large amount of Ce by the formation of Ce-containing phases (Al_3Ce and $Al_7Si_{3.5}Cu_{3.5}Ce$), the refinement of Ce on Al-Si eutectic phase is suppressed, resulting in the reprecipitate of the phases.

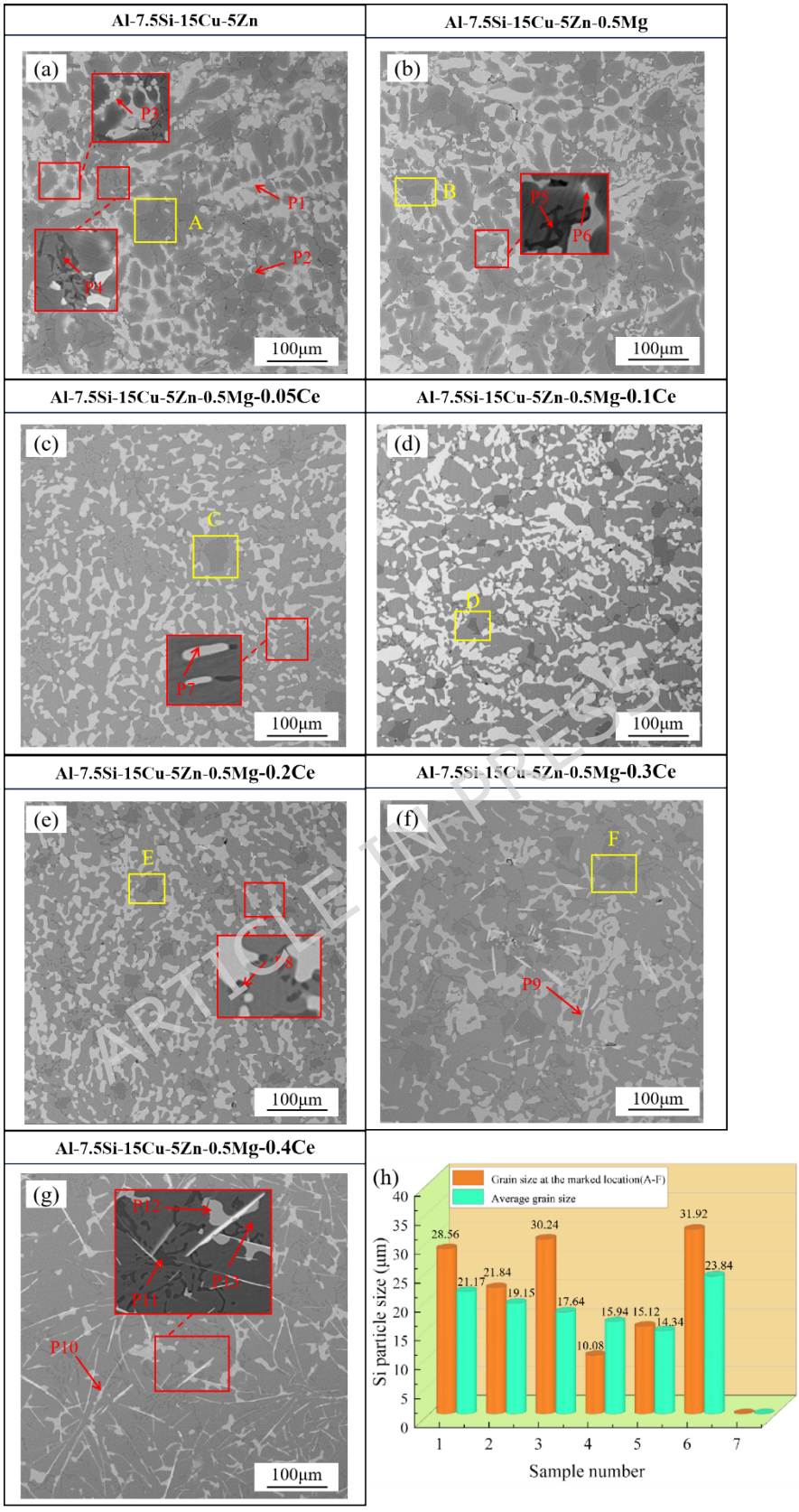

Fig. 6 (a-g)Microstructure of brazing alloys; (h) Primary Si particle size in microstructure of brazing alloys

Table 3 EDS results of phase composition for P1-P13 in Fig. 6

Mark Points	Al	Si	Cu	Mg	Zn	Ce	Possible phase
P1	63.81	—	36.19	—	—	—	Al_2Cu
P2	1.84	98.16	—	—	—	—	Si particle
P3	69.06	—	—	—	30.94	—	Al-Zn
P4	85.19	14.81	—	—	—	—	Al-Si eutectic
P5	87.35	12.65	—	—	—	—	Al-Si eutectic
P6	70.27	—	—	—	29.73	—	Al-Zn
P7	74.16	—	—	—	—	25.84	Al_3Ce
P8	87.17	12.83	—	—	—	—	Al-Si eutectic
P9	53.86	18.23	18.97	—	—	8.94	$Al_7Si_{3.5}Cu_{3.5}Ce$
P10	53.64	17.91	18.36	—	—	10.09	$Al_7Si_{3.5}Cu_{3.5}Ce$
P11	88.72	11.28	—	—	—	—	Al-Si eutectic
P12	67.23	—	32.77	—	—	—	Al_2Cu
P13	98.16	0.63	—	—	1.21	—	α-Al

3.3 Microstructure of brazed joints

Fig. 7 shows the cross section morphology of the brazed joints using the seven brazing alloys, and the EDS analysis results of points P1-P18 marked in the figure are presented in Table 4. The brazing alloys are found to tightly bond the base material, without evident cracks in the joints. The polished brazed joints show a distinctive structure consisting of the brazing alloy layer and an interface zone on 5083 aluminum base alloy. Using the Image-Pro software, the interface layer was defined as the region extending from where diffusion becomes evident in the brazing filler layer to the surface of the 5083 substrate. Its thickness represents the bonding state between the brazing alloy and the base alloy, which influencing the mechanical properties of the joints[35][36].

Fig. 7 (a) shows the phase composition in the brazing alloy layer

consists of α-Al phase (P1), Al_2Cu phase (P2), and a supersaturated solid solution (P3) formed by the dissolution of Mg and Si in α-Al (Mg originates from the diffusion within the base material). In the interface zone, there are new-formed phases like Mg_2Si (P4) and $Al_6(Fe,Mn)$ (P6) in addition to the Al_2Cu (P5), which can be referred to as the intermetallic compounds (IMCs). Fig. 8 (a) shows the EDS mapping results of the microstructure of the joints. The element diffusion reaction in the interface zone mainly occurs on the side close to the brazing alloy layer, with some Cu elements diffusing into the middle of the interface zone, forming elongated Al_2Cu phases (P7). The interface zone is 86.54 μm and exhibits some tiny pores at Al. Such pores forms due to the trapped gases such as O_2, N_2, and H_2 in melt during brazing, which cannot escape after solidification in brazed joints[37]. The formation of pores may cause a degraded mechanical stability.

For the joint using the brazing alloy with 0.5 wt.% Mg in Fig. 7 (b), the phase composition of the brazing alloy layer is consistent with that of the Al-7.5Si-15Cu-5Zn brazed joint, but the morphology of the Al_2Cu phase changes from bulks to bands, as indicated by red arrow, due to that Mg elements can alter the distribution of Cu along the α-Al grain boundaries[38], thereby changing the structure of the Al_2Cu phase (P8), which is also the reason for the presence of a small amount of Mg in the EDS results of the Al_2Cu phase. The interface zone thickness of the brazed joint decrease to 80.21 μm, which is comparable to that of the Al-7.5Si-15Cu-5Zn brazed joint. In this zone, IMCs (Mg_2Si-(P9), $Al_6(Fe, Mn)$-(P10) and Al_2Cu-(P11)) can be observed. However, the EDS mapping results in Fig. 8 (b) show that the amount of IMCs decreases because the increase in Mg content intensifies the clustering behavior of Cu in the brazing alloy layer[39]. Meanwhile due to the dynamic solidification process of

welding[40], Cu with lower diffusion coefficient does not have enough time to diffuse to the interface zone. In addition, pores (B1) become more evident in the interface zone and they also exist in the brazing alloy (B2). The formation of the pores can also be attributed to the evaporation of some Mg element during brazing process in addition to the trapped gases[41].

For the joints with 0.05-0.2 wt.% Ce in the brazing alloys, the phase composition of the brazing alloy layer remains unchanged. As the Ce content increases, the morphology of the Al_2Cu phase gradually becomes band-like. When the Ce content reaches 0.2 wt.%, the structure of some Al_2Cu phases in the brazing alloy appears fragmented (P13). According to the EDS results at point P13, some Ce is dissolved inside the Al_2Cu phase, occupying the sites inside the Cu atoms, thereby altering the morphology of the Al_2Cu phase[42]. For the interface zone, its thickness gradually decrease with increasing Ce content because during solidification of brazing alloy, Ce limits the diffusion of Cu from the brazing layer to the interface zone[43], resulting a thin interface zone. Thus, at 0.2 wt.% Ce content, the thickness of the interface zone reaches a minimum value of 51.63 μm. The EDS maps in Fig. 8 (c) shows an evident diffusion of Cu elements to the interface zone. For these joints, pores are greatly eliminated after Ce addition. Pores were assessed qualitatively from cross-sectional micrographs. Due to Ce-induced undercooling, the residence time of gas in the melt is shortened, making it easier to escape. From Fig. 7 (d) and 7 (e), it can be seen that the pores in the interface region almost disappear compared to Fig. 7 (c) (pores in C1).

As Ce content exceeds 0.2 wt.%, the basic phase composition of the brazing alloy layer remains unchanged, but the effect of Ce on the evolution of Al_2Cu phase gradually weakens. Meanwhile, the

needle-like AlSiCuCe phases appear in the brazing alloy layer. For the interface region, the presence of needle-like phases can also be observed, meaning that the influence of Ce on the undercooling of the melt becomes insignificant and the thickness of the interface zone increases. As shown in Fig. 7 (f) and 7 (g), pores reappear at the interface zones at D1 and E1. According to reports, a higher quantity and more complex morphology of IMCs in the interfacial zone of brazed joints tend to result in an increased thickness of this zone. These IMCs are prone to act as preferential sites for crack initiation and propagation, leading to joint failure and a reduction in strength[44][45]. The acicular phase within the interfacial region is more prone to become the starting point for crack initiation. Therefore, the brazed joint using Al-7.5Si-15Cu-5Zn-0.5Mg-0.2Ce brazing alloy is believed to exhibit the highest tensile strength.

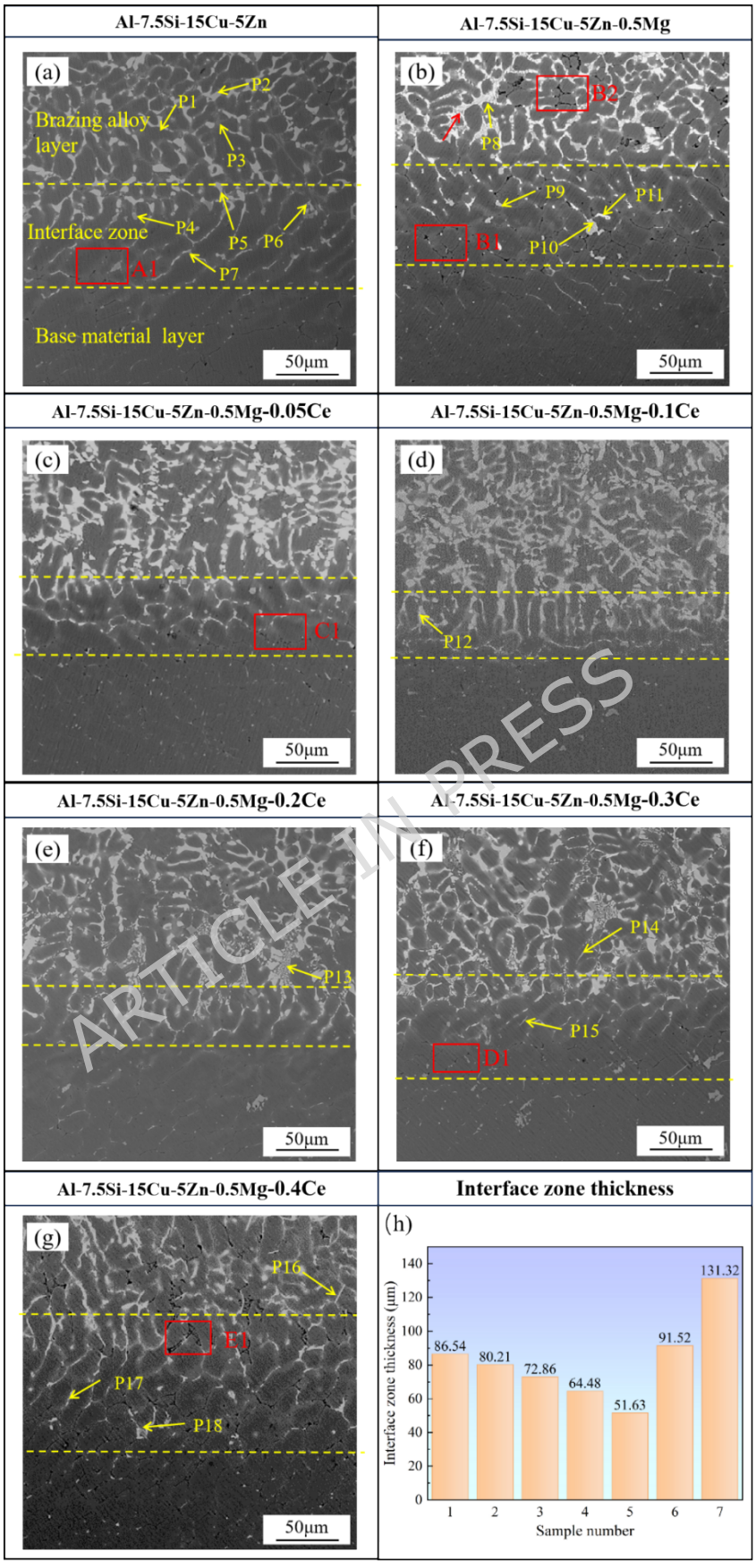

Fig. 7 (a)-(f)Microstructure of brazed joints; (h) Interface zone thickness

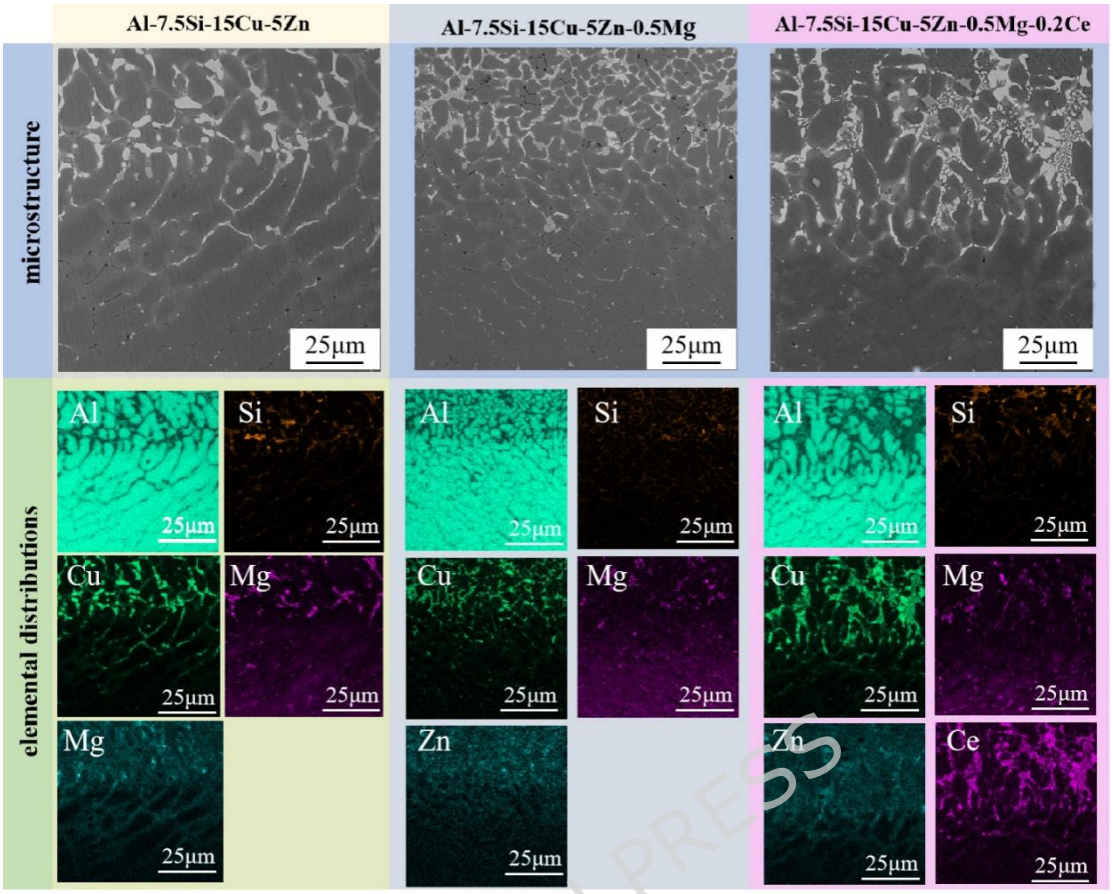

Fig. 8 EDS surface scanning results of brazed joints

Table 4 EDS results at points P1-P18 in Fig. 7

Mark Points	Al	Si	Cu	Mg	Zn	Fe	Mn	Ce	Possible phase
P1	96.05	1.34	—	—	2.61	—	—	—	α-Al
P2	65.23	1.06	33.71	—	—	—	—	—	Al_2Cu
P3	67.05	16.10	—	16.03	0.82	—	—	—	Supersaturated solid solution
P4	22.75	32.54	—	44.71	—	—	—	—	Mg_2Si
P5	64.8	—	35.1	—	—	—	—	—	Al_2Cu

	3		7					
P6	80.76	3.24	2.38	—	—	7.69	5.93	—	$Al_6(Fe,Mn)$
P7	67.83	—	32.17	—	—	—	—	—	Al_2Cu
P8	67.99	—	28.04	3.97	—	—	—	—	Al_2Cu
P9	19.06	34.78	—	46.16	—	—	—	—	Mg_2Si
P10	81.75	—	—	1.32	—	7.54	9.39	—	$Al_6(Fe,Mn)$
P11	66.58	—	30.75	2.67	—	—	—	—	Al_2Cu
P12	80.78	—	2.22	—	—	8.28	8.72	—	$Al_6(Fe,Mn)$
P13	64.37	—	32.61	—	—	—	—	3.02	Al_2Cu
P14	56.84	15.74	17.75	—	—	—	—	9.67	$Al_7Si_{3.5}Cu_{3.5}Ce$
P15	52.67	19.34	18.92	—	—	—	—	9.07	$Al_7Si_{3.5}Cu_{3.5}Ce$
P16	53.92	20.19	17.36	—	—	—	—	8.53	$Al_7Si_{3.5}Cu_{3.5}Ce$
P17	54.48	19.83	17.07					8.62	$Al_7Si_{3.5}Cu_{3.5}Ce$
P18	81.93	—	—	—	—	9.26	8.81	—	$Al_6(Fe,Mn)$

4 Mechanical properties of brazed alloys and joints

4.1 Theoretical prediction

To theoretically predict the mechanical properties of the Al-7.5Si-15Cu-5Zn-0.5Mg-xCe brazing alloys, the stiffness matrix is calculated using the Materials Studio software to obtain the elastic constants (C_{11}, C_{12} and C_{44}) and the bulk modulus (B), Young's modulus (E), and shear modulus (G) of the alloys. The results are shown in Table 5. For cubic crystals, high mechanical stability needs to fulfill the criteria of $C_{11}>0$, $C_{44}>0$, $C_{11}-C_{12}>0$ and $C_{11}+2C_{12}>0$. From Table 5, all Al-7.5Si-15Cu-5Zn-0.5Mg-xCe brazing alloys satisfy the criteria, suggesting that this brazing material system exhibits high mechanical stability.

Table 5 The elastic constant (C_{ij}), bulk modulus (B), shear modulus (G), Young's modulus (E), Poisson's ratio (ν), B/G ratio, and Cauchy pressure of brazing alloys.

Sample number	C_{11}	C_{12}	C_{44}	B	E	G	C_{12}-C_{44}	B/G	ν
	These Units Are All GPa								
1	438.6	188.9	101.1	272.1	290.8	110.0	87.8	2.474	0.322
2	434.7	196.4	107.5	277.5	296	111.4	88.9	2.462	0.321
3	433.3	200.8	110.6	278.3	298.2	112.8	90.2	2.467	0.321
4	432.9	204.2	113.8	280.4	301.2	114.0	90.4	2.460	0.321
5	429.9	210.9	119.2	283.9	304.5	115.2	91.7	2.463	0.321
6	400.2	214.9	125.3	276.7	293.8	111.0	89.6	2.492	0.323
7	380.7	218.4	130.5	272.5	285.9	107.7	87.9	2.526	0.325

The changes in bulk modulus (B), Young's modulus (E), and shear modulus (G) of Al-Si-Cu-Zn-Mg-*x*Ce are shown in Fig. 9 (a).The addition of Mg and Ce to the Al-Si-Cu-Zn brazing alloy results in an initial increase followed by a decrease in the bulk modulus (B), Young's modulus (E), and shear modulus (G). This behavior can be attributed to Mg and Ce elements induce phase transformations and refine the microstructure of the alloy. At a Ce content of 0.2 wt.%, the Young's modulus (E) and shear modulus (G) of the brazing alloy reached their maximum values of 304.5 GPa and 115.2 GPa, respectively. The shear modulus reflects the material's response to shear stress and is generally indicative of the alloy's hardness, which is related to its incompressibility. The bulk modulus is influenced by the characteristics of atomic bonds within the material. Materials with higher strength exhibit greater bulk and shear modulus[46]. Thus, adding an appropriate amount of Mg and Ce to the alloy can enhance the strength and hardness of the brazing alloy.

Fig. 9 (b) illustrates the spatial distribution of the Young's modulus to visualize the effect of Mg and Ce contents on the brazing alloy. A narrower range of Young's modulus distribution indicates greater structural stability. For the Al-7.5Si-15Cu-5Zn brazing alloy system, the non-spherical spatial distribution of the modulus suggests an anisotropic crystal structure and the range is quite large. With 0.5 wt.% Mg, the Al-7.5Si-15Cu-5Zn-0.5Mg brazing alloy exhibits a decreased range of Young's modulus distribution, indicating the structural stability improved. Meanwhile, the crystal structure transforms from anisotropic to isotropic. Ce can further decrease the range and a minimum of 2.2 GPa is achieved for the brazing alloy at a Ce content of 0.2 wt.%, indicating the highest structural stability. However, when the Ce content exceeds 0.2 wt.%, the crystal structure of the brazing alloys transforms from isotropic

to anisotropic, and the modulus range increases again, leading to a degraded structural stability.

Fig. 10 (a) shows the ratio of bulk modulus to shear modulus (B/G) and Poisson's ratio (ν) for the brazing alloys. At B/G≥1.75 and ν≥0.26, a material exhibits ductility[47], otherwise, it is brittle. From Fig. 10 (a), the B/G and ν values of the multicomponent brazing alloy systems exhibit ductility. Fig. 10 (b) illustrates the trend in Cauchy pressure (C_{12}-C_{44}) for the brazing alloys. A higher Cauchy pressure indicates greater structural stability and better ductility. In Fig. 10 (b), the addition of Mg and Ce elements in the brazing alloy causes an increase of the Cauchy pressure. With Ce, it initially increases and then decreases and reaches the maximum value of 91.7 GPa at 0.2 wt.% Ce, indicating that the Al-7.5Si-15Cu-5Zn-0.5Mg-0.2Ce brazing alloy possesses the optimal ductility and structural stability.

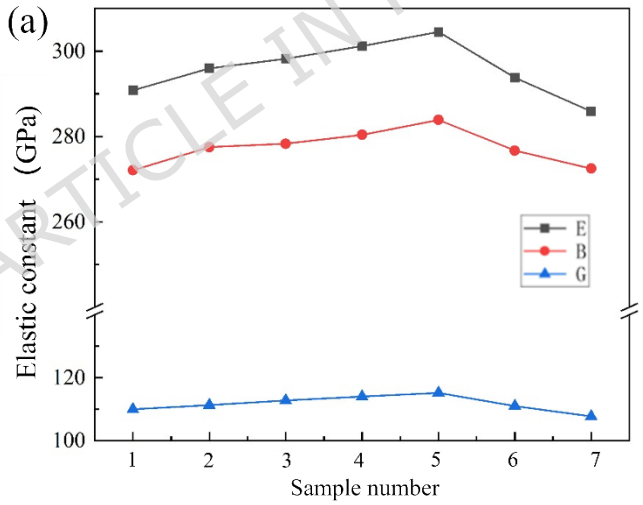

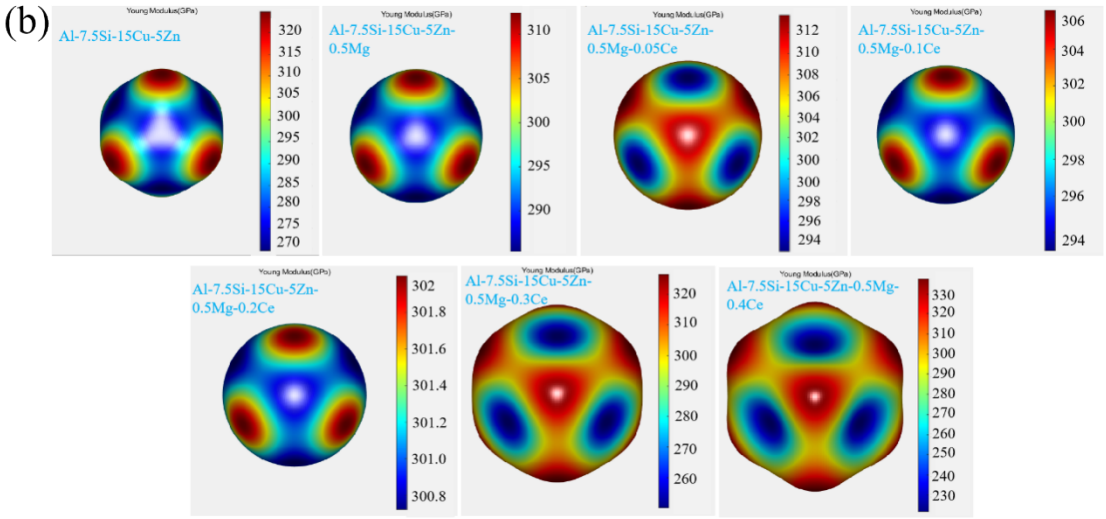

Fig. 9 (a) Elastic constant of brazing alloy)(GPa); (b) Spatial distribution of the Young's modulus(GPa)

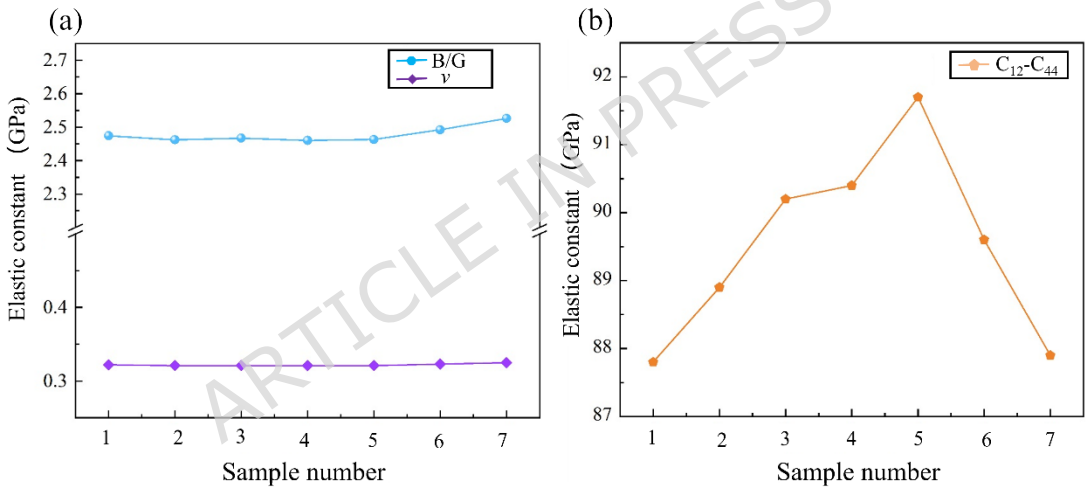

Fig. 10 Elastic constant (GPa)

4.2 Measured mechanical properties

Fig. 11 shows the results of the mechanical performance of joints using the brazing alloys. For the tensile strength in Fig. 11 (a), the addition of Mg and Ce in the Al-7.5Si-15Cu-5Zn brazing alloy results in an increase of tensile strength of the joints, consistent with the first-principles calculations for bulk modulus (B) and shear modulus (G). With Ce, the tensile strength of the joints initially increases and then decreases, reaching a maximum value of 261.14 MPa for the

joints using the 0.2 wt.% Ce brazing alloy. It exhibits a significant improvement in joint strength compared to joints brazed using conventional Al-Si brazing alloys on 5xxx series aluminum alloys (125 MPa)[48].

For the joints using Al-7.5Si-15Cu-5Zn-0.5Mg brazing alloy, the tensile strength is found improved compared with the joints without addition of 0.5 wt.% Mg. Such improvement can be attributed to the thinner interface zone which decreases the impact of stress concentration at the interface on tensile strength. In addition, the band-like morphology of Al_2Cu phases (Fig. 7 (b)) releases the stress and makes the phases tightly cross-linked to improve the tensile strength of the joint.

When 0.05-0.2 wt.% Ce is added to the brazing alloy, the tensile strength of the corresponding joints gradually increases, which can be attributed to the stress release in the joints due to the less IMCs and elimination of pores (Fig. 7 (c-e)). On the other hand, the fragmented Al_2Cu particles (Fig.7 (e)) can absorb strain[49], thereby enhancing the tensile strength of the joint. When the Ce content is 0.2 wt.%, the brazed joint exhibits a reduced number of intermetallic compounds at the interface, with pores essentially eliminated and the interface thickness minimized. The joint experiences less stress concentration and demonstrates optimal tensile strength. When the Ce content exceeds 0.2 wt.%, the AlSiCuCe needle-like phase and pores in the interface zone might intensify stress concentration, leading to the decreased tensile strength.

Fig. 11 (b) shows the microhardness variation from both ends of 5083 aluminum alloy base material to the weld center. The microhardness at the weld center is higher than that of the base material, which can be attributed to the formation of the Al_2Cu phase and the supersaturated solid solution. The microhardness in the

interface zone is highest benefiting from the formation of IMCs. At 0.5 wt.% Mg and 0.05-0.2 wt.% Ce, the number of IMCs in the interface zone is relatively small, resulting in the lower microhardness compared to other joints. At higher Ce, the needle-like AlSiCuCe IMCs in the interface zone (Fig. 7(f) and (g)) exhibit high hardness, leading to an increased average microhardness of the joints. However, the pores might decrease the microhardness. When Ce content reaches 0.2 wt.%, the microhardness of the joint reaches the biggest about 194.6 $HV_{0.2}$, which can be attributed to the reduction of pores[50].

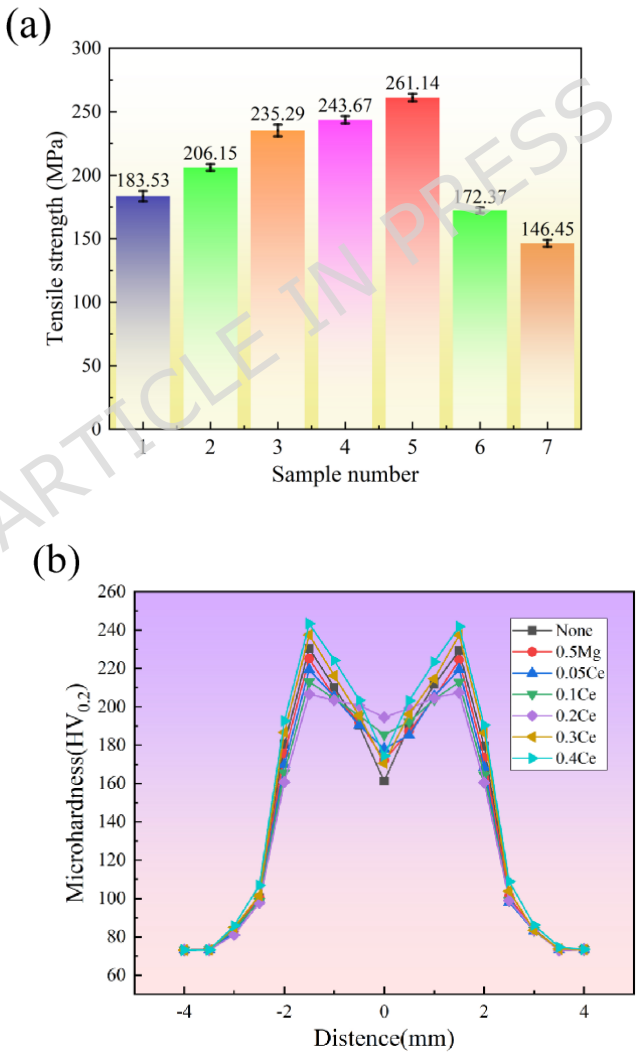

Fig. 11 Mechanical properties of brazed joints (a) Tensile strength; (b) Microhardness

4.3 Fracture property

Fig. 12 shows the elongation of brazed joints after tensile testing. Compared to the Al-7.5Si-15Cu-5Zn brazing alloy, the elongation slightly increased after adding 0.5 wt.% Mg, which can be attributed to the reduction of IMCs in the interface zone and the refinement of the Al_2Cu phases in the brazing alloy layer. However, the local defects caused by the pores easily lead to stress concentration during the tensile process, sacrificing the plastic deformation capacity of the joint. When adding 0.05-0.2 wt.% Ce, the defects are eliminated and the Al_2Cu phases become delicate, resulting in the improved elongation after and reaching a maximum value of 11.95 % when the Ce content is 0.2 wt.%. When the Ce content exceeds 0.2 wt.%, defects and the formation of needle-like phases within the weld result in a large number of local stress concentrations during the tensile process, causing a significant decrease in elongation after fracture.

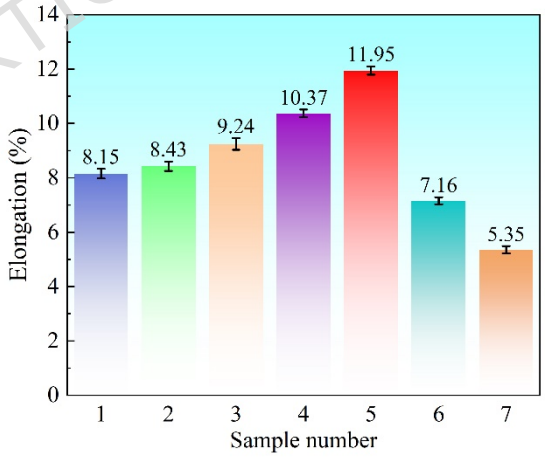

Fig. 12 Elongation after fracture of brazed joints

Fig. 13 presents the fracture morphologies of the brazed joints, and the EDS analysis results of points P1-P6 marked in the figure are presented in Table 6. When the Ce content does not exceed 0.2 wt.%, fracture occurs at the interfacial region or in areas close to the base

metal. When the Ce content exceeds 0.2 wt.%, the fracture location shifts to the brazing alloy layer. For the Al-7.5Si-15Cu-5Zn brazing alloy, the brazed joint exhibits a ductile-brittle fracture. The fracture initiates and rapidly propagates along the Al_2Cu phase (P1), exhibiting cleavage surfaces on the brittle fracture. Pores at the interface weakens the bonding strength between the brazing alloy and the base material, facilitating the initiation of fracture. Additionally, a few ductile dimples can be observed in Fig. 13 (a), developed by the precipitation of the Mg_2Si phase (P2).

After adding 0.5 wt.% Mg, the fracture is also in a mixed mode of ductile-brittle. The initiation of fracture also occurs at the pores and Al_2Cu phases. However, due to the refinement of Al_2Cu phases (band-like morphology in Fig 7 (b)), the number of cleavage surfaces formed after Al_2Cu fracture is reduced, improving the elongation.

When Ce is added in the range of 0.05-0.2 wt.%, pores within the fracture surface gradually decrease and fracture mainly propagates along the Al_2Cu phase. However, as the Ce content increases, the Al_2Cu phase gradually fractures, resulting in greater plastic deformation[51]. This results in larger ductile dimples, as shown in Fig. 13 (e), a larger number of ductile dimples can be observed, which contributes to the increase in elongation. When the Ce content exceeds 0.2 wt.%, no noticeable ductile dimples are observed in the fracture surface, indicating a brittle fracture. The pores and Al_2Cu phase (P3 and P6) leads to more cleavage surfaces in the fracture. On the other hand, the AlSiCuCe needle-like phases (P4 and P5) at the interface might causes stress concentration to initiate the fracture and it propagates rapidly along these needle-like phases, forming larger cleavage surfaces and resulting in a decrease in post-fracture elongation. Overall, as the Ce content increases, the fracture behavior of the joint evolves from a mixed ductile-brittle

mode to a brittle-dominated fracture.

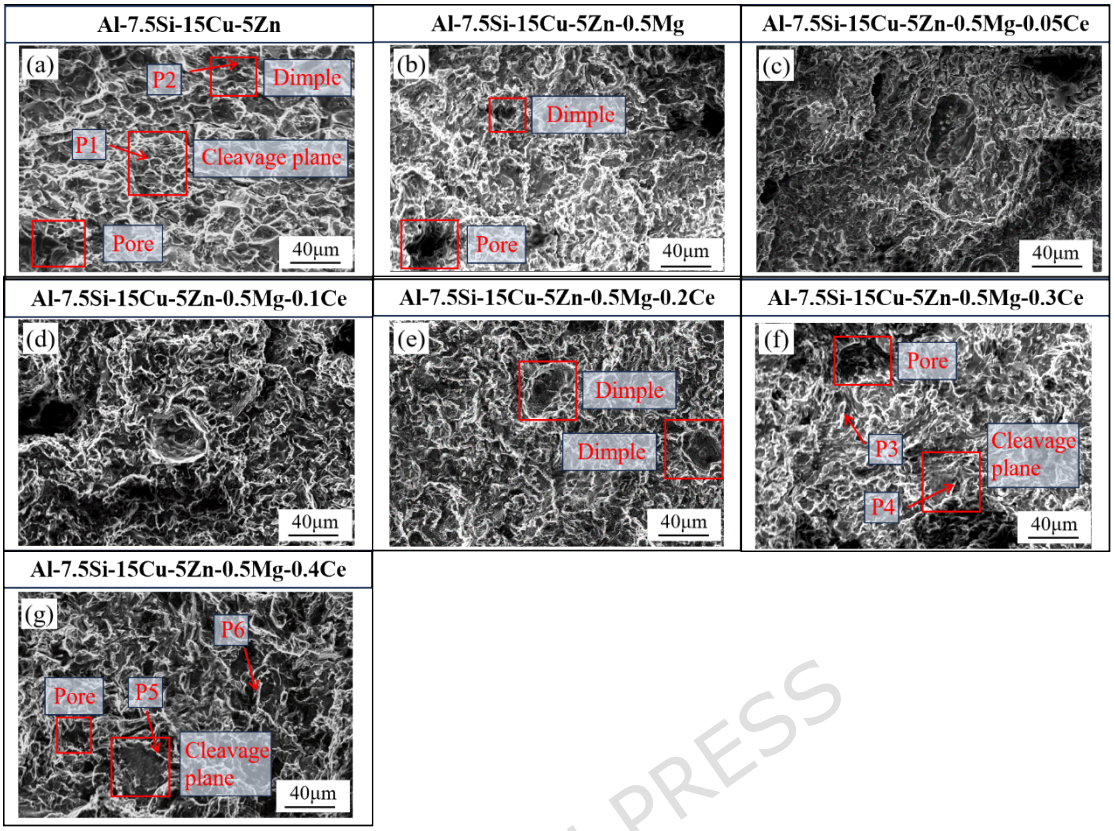

Fig. 13 Fracture morphology of brazed joints

Table 6 EDS results at the marked locations in Fig. 13

Mark Points	Al	Si	Cu	Mg	Ce	Possible phase
P1	65.04	—	34.96	—	—	Al_2Cu
P2	28.39	25.17	—	46.44	—	Mg_2Si
P3	66.47	—	32.58	—	0.95	Al_2Cu
P4	54.76	16.73	19.24	—	9.27	$Al_7Si_{3.5}Cu_{3.5}Ce$
P5	52.14	17.27	20.76	—	9.83	$Al_7Si_{3.5}Cu_{3.5}Ce$
P6	68.21	—	31.79	—	—	Al_2Cu

5 Conclusions

This study investigated the effects of adding 0.5 wt.% Mg and varying Ce content (x=0.05, 0.1, 0.2, 0.3, 0.4 wt.%) on the melting behavior of the Al-7.5Si-15Cu-5Zn brazing alloy and the microstructure of the corresponding joints for welding 5083

aluminum alloy. Both first-principles calculations and experiments were employed to evaluate the mechanical properties of the brazed joints.

The results indicate that the addition of Mg and Ce shortens the melting interval of the base alloy. Specifically, with 0.2 wt.% Ce, the brazing alloy achieves the lowest melting point and narrowest melting interval, measured at 515.8 °C and 49.1 °C, respectively. Microstructural analysis reveals that Mg and Ce additions refine the microstructure. However, excessive Ce (above 0.2 wt.%) leads to the formation of needle-like $Al_7Si_{3.5}Cu_{3.5}Ce$ phases. While Mg addition tends to induce porosity in both the filler alloy and the joints, optimal refinement and a delicate microstructure are obtained at 0.2 wt.% Ce.

First-principles calculations predict that Mg and Ce enhance the strength and hardness of the joints. The calculations suggest that the composition with 0.5 wt.% Mg and 0.2 wt.% Ce should yield the best mechanical performance. Experimental results confirm this prediction: joints brazed with the Al-7.5Si-15Cu-5Zn-0.5Mg-0.2Ce alloy exhibit the highest tensile strength and microhardness, reaching 261.14 MPa and 194.6 $HV_{0.2}$, respectively. Furthermore, for this optimal joint, fracture surface analysis indicates a mixed ductile-brittle mode. The improvement in elongation is attributed to the elimination of pores and significant microstructural refinement.

Acknowledgements

This work was financially supported by Foundation of Research Project of China (50904010201) and Doctoral Scientific Research Foundation of Hubei University of Automotive Technology (BK202482).

Author contributions

Yan Wang: Proposing the research topic: designing the research plan; finalizing the paper.

Yuechao Zhuo: Reviewing and organizing literature, designing the paper framework; drafting the paper, revising the paper.

Zhe Sun: Statistical analysis; guidance and support.

Conghui Zhang: Statistical analysis; technical and material support.

Yonglin Zhao: Statistical analysis, acquiring research funding, technical and material support.

Bingyuan Han: Reviewing and finalizing the paper.

Yuxiang Liu: Statistical analysis; finalizing the paper.

Conflicts of interest or competing interests

The authors declare that they have no known competing financial interests or personal relationships that could have appeared to influence the work reported in this paper.

Data and code availability

The datasets used or analyzed during the current study available from the corresponding author on reasonable request.

Supplementary information

Not Applicable

Ethical approval

Not Applicable

References

[1] Wu LJ, Han XH, Ma GL (2023) Effects of welding layer arrangement on microstructure and mechanical properties of gas metal arc welded 5083/6005A aluminium alloy butt joints. Transactions of Nonferrous Metals Society of China 9:1665-1676.

[2] Huang YM, Yuan YX, Feng YC (2022) Effect of activating flux CrO on microstructure and properties of laser welded 5083 aluminum

alloys.Optics & Laser Technology 150:107930.

[3] Chen JL, Ye B, JIANG H Y (2021) Effects of Ni on the Microstructure and Mechanical Properties of Al-Si-Cu-Ni-Mg Hypereutectic Piston Alloy. Hot Working Technology 4:32-37.

[4] Gao Z, Jin XW, Li SQ (2024) Study on microstructure and mechanical properties of 3003 aluminum alloy joints brazed with Al–Si–Cu–Ni paste brazing materials. Scientific Reports 14:10648.

[5] Peng CY, Zhu DD, Li KF (2021) Research on a low melting point Al-Si-Cu (Ni) filler metal for 6063 aluminum alloy brazing. Applied Sciences 9:4296.

[6] Du X, Zhao F, Peng C (2023) Effect of Sr on the microstructure and properties of Al-6.5Si-20Cu-1.5Ni filler metal for brazing 6063 aluminum alloy. Welding in the World 67:2039–2048.

[7] Chen B, Wang FZ, Ren SM (2023) Influence of erbium addition on microstructure and performances of AlSi10Mg alloy prepared by selective laser melting. Journal of Rare Earths 3:659-681.

[8] Dong XB, Guo YC, Li JP (2022) Effect of ultrasonic vibration on solidification microstructure in near-eutectic Al-Si piston alloy. Rare Metal Materials and Engineering 1:11-17.

[9] NIU ZW, HUANG JH, XU FZ (2016) Research Status and Prospects of Hard Brazing Materials for Aluminum and Aluminum Alloy Brazing. Transactions of Nonferrous Metals Society of China 1:77-87.

[10] SUNIL M, PRADHAN A (2022) Effects of melt thermal treatment on cast Al-Si alloys: A review. Materials Today: Proceedings 62: 6568-6572.

[11] Niu ZW, Huang JH, Liu KK (2017) Analysis of microstructure and properties of 6061 aluminum alloy joint brazed with Al-Si-Ge-Zn brazing material. Transactions of The China Welding Institution 9:97-101.

[12] Dai W, Xue SB, Lou JY (2012) Microstructure and Properties of 6061 Aluminum Alloy Brazing Jointwith AlSiZn Filler Metal. Materials Transactions 9:1638-1643.

[13] CHUANG TH, TSAO L C, TSAI T C (2000) Development of a low-melting-

point filler metal for brazing aluminum alloys. Metallurgical and Materials Transactions A 9:2239−2245.

[14]Suresh C, Shivam B, Khushboo R (2022) Development and characterization of Al-Si-Cu-Zn-Sn brazing filler alloy using vacuum arc furnace. Materials Today: Proceedings 14:7547-7553.

[15]Emad H, Calin D, Ghada S (2024) Effects of grain boundary chemistry and precipitate structure on intergranular corrosion in Al-Mg-Si alloys doped with Cu and Zn. Corrosion Science 236:112227.

[16]Lu Y, Wen SP, Gao KY (2024) The phase transformation and enhancing mechanical properties in high Zn/Mg ratio Al–Zn–Mg–Cu(-Si) alloys. Journal of Materials Research and Technology 31:1693-1702.

[17]Li Q, Li B, Li J (2017) Effects of the addition of Mg on the microstructure and mechanical properties of hypoeutectic Al–7%Si alloy. International Journal of Metalcasting 4:823-830.

[18]Musa Y, Dursun Ö (2013) The effects of Mg amount on the microstructure and mechanical properties of Al-Si-Mg alloys. Materials and Design 51:767-774.

[19]Ye KF, Cai XL, Sun B (2023) Effect of rare earth Ce on the microstructure and mechanical properties of cast Al–7Si alloys. Journal of Science: Advanced Materials and Devices 4:623-631.

[20]Sezgin C, Hisham A, Mattias T (2023) Effect of Ce addition on microstructure, thermal and mechanical properties of Al-Si alloys. Materials Today Communications 34:518-529.

[21]Bevilaqua WL, Stadtlander AR, Froehlich AR (2020) High-temperature mechanical properties of cast Al-Si-Cu-Mg alloy by combined additions of cerium and zirconium. Materials Research Express 7:026513.

[22]Nguyen DN, Bui TM, Vu A, Sai MT, Pham MK, Tran DH (2022) Properties of Al-Z-Mg-Cu alloy when modified by La, Ce and thermo-mechanical treatment. Acta Metallurgica Slovaca 28(2):142–151.

[23]Gao Y, Qiao JL, Wu DT (2020) First principle calculation of the effect of

Cr, Ti content on the properties of VMoNbTaWMx (M = Cr, Ti) refractory high entropy alloy. Vacuum 179:109459.

[24]Wu YN, Liu JS, Zhang Y (2024) First-principles calculation for mechanical properties of TiZrHfNbTa series refractory high-entropy alloys. Materials Today Communications 40:110165.

[25]Jiang DY, Xie LC, Wang LQ (2023) Current application status of multi-scale simulation and machine learning in research on high-entropy alloys. Journal of Materials Research and Technology 6:1341-1374.

[26]Chen L, Hao XH, Wang YY (2020) First-principles calculation of the effect of Ti content on the structure and properties of TiVNbMo refractory high-entropy alloy. Materials Research Express 7:106516.

[27]KLAVER T, CHEN JH (2003) Density functional theory study of alloy element interstitials in Al. Journal of Computer-Aided Materials Design 10:155-162.

[28]Yu Z, Bo W, Shicheng W (2022) Estimation of mechanical properties of Mg-5Zn-0.5Al-xSn alloy based on virtual crystal approximation. Heliyon 8:e11224-e11229.

[29]AE M, R A, PA S (2006) Nonequivalence of the generalized gradient approximations PBE and PW91. Physical review, B. Condensed matter and materials physics 73:5123-1-5123-7.

[30]Alharbi FF, Shahid M, Zahid A (2023) First principles calculation to investigate the effect of Mn substitution on Cu site in CeCu3-x Mn x V4O12 (x = 0, 1, 2 and 3) system. RSC advances 13:12973-12981.

[31]Frank C, Babak S (2023) Aluminum Cast Alloys Based on the Al-Ce-Si-Mg System: An Influence of Silicon on Crystallization, Phase Composition, and Tensile Properties. Metallurgical and Materials Transactions A 53:4233-4246.

[32]Li HX，Feng YD，Shen WJ (2022) Microstructure and mechanical properties of Cu/Al joints brazed using (Cu, Ni, Zr, Er)-modified Al—Si filler alloys. Transactions of Nonferrous Metals Society of China 32:3623-

3634.

[33]Niu GD, Wang Y, Mao J (2024) Characterization of L12-Al3Ce phase and its purification mechanism in the Al-Ce-TiCN alloy. Materials Characterization 217:114425.

[34]Wang J, Cui J, Ma L (1993) Interaction Intensity of Alloying Elements and its Application in As-Cast Aluminum Alloys with Rare Earth Additions. Xi'an Inst. Metall. Cons. Eng 4:445-449.

[35]Qiu YX, Huang ZR, Lin ZY (2024) Interfacial strength saturation due to local melting at bonding interface in ultrasonic welding of 7075 aluminum alloy to 316L stainless steel. Materials Letters 362:136249.

[36]Xie J, Tang L, Gao P (2025) Effects of Ni addition on wettability and interfacial microstructure of Sn-0.7 Cu-xNi solder alloy[J]. Soldering & Surface Mount Technology, 37(2): 86-96.

[37]Saifudin, Nurul M, Eko S (2024) Effect of vibration frequency on mechanical properties and microstructure of metal inert gas welded dissimilar AA5083 and AA6061 aluminum alloy joints. Results in Engineering 24:102970.

[38]Yang HB, Liu YT, Li Y (2024) Influence of Cu/Mg ratio and content on heat-resistance of Al-Cu-Mg alloys. Journal of Materials Research and Technology 29:1040-1051.

[39]Chen YF, Sun YN, Cheng WJ (2024) Effect of Mg content on Cu precipitation behavior in Al-Cu-Mg ternary alloy by molecular dynamics simulation. Computational Materials Science 236:112952.

[40]Wu D, Cai XL, Li HM (2025) Interface characteristics and mechanical behavior of aluminum alloy/ultrahigh-strength steel plasma arc welded joint. Journal of Materials Research and Technology 34:1057-1067.

[41]Cheolho Park. Hyunbin Nam, Namhyun Kang (2024) Effect of welding current on the mechanical properties of Al 5083 alloy processed using high-current gas metal arc welding. Journal of Advanced Joining Processe 10:100240.

[42]Niu GD, Zhu LJ, Ren WR (2023) Elevated temperature microstructural stability in Al-7Cu-0.5Mn-0.2Zr alloys through Ce addition: Enhanced coherent interfacial stability of cu-rich θ’/α-Al interface. Materials Characterization 200:112908.

[43]Chen SY, Li Q, Zhong J (2019) On diffusion behaviors in face centered cubic phase of Al-Co-Cr-Fe-Ni-Ti high-entropy superalloys. Journal of Alloys and Compounds 791:255-264.

[44]Xia MY, Zhou DJ, Gao ZM (2024) Study on the structural transformation of 6xxx composite four-layer aluminum alloy sheet during brazing and artificial aging and its influence on strengthening and corrosion behavior. Corrosion Science 229:111886.

[45]Li T, Chen Y, Xiong J (2025) Different interfacial layer states, microstructure evolution, and mechanical properties during aging treatment of two coatings fabricated by TIG surfacing and laser cladding[J]. Materials Characterization 32: 115842.

[46]Ru JD, Ma R, Wan PM (2022) First principles calculation on electronic structures and mechanical properties of TiCrTaV high–entropy alloy. Materials Today Communications 31:103801.

[47]Li YR, Zhang SH, Gong CW (2024) A comprehensive investigation of alloying elements on site preferences, elastic properties and electronic structure of Mg17Al12 by first-principles calculations. Vacuum 227:113450.

[48]Song JL, Lin SB, Yang CL, Fan CL (2009) Effects of Si additions on intermetallic compound layer of aluminum–steel TIG welding–brazing joint. Journal of Alloys and Compounds 488:217–222.

[49]Peng ML, L C, Wei H (2024) Study on the mechanism of improvement of mechanical properties of Al-Mg-Si aluminum alloys by Cu and Ce. Journal of Materials Research and Technology 33:3790-3808.

[50]Li JY, Huang Y, Chen CF (2024) The structural stability and mechanical properties of doped Al2Cu precipitates with different elements by first-

principles calculations. Computational Condensed Matter 41:e00957.

[51]Zhang Y, Li RQ, Chen PH (2019) Microstructural evolution of Al2Cu phase and mechanical properties of the large-scale Al alloy components under different consecutive manufacturing processes. Journal of Alloys and Compounds 808:151634.